Noise in Current-Commutating CMOS Mixers

Manolis T. Terrovitis, *Student Member, IEEE*, and Robert G. Meyer, *Fellow, IEEE*

***Abstract*— A noise analysis of current-commutating CMOS mixers, such as the widely used CMOS Gilbert cell, is presented. The contribution of all internal and external noise sources to the output noise is calculated. As a result, the noise figure can be rapidly estimated by computing only a few parameters or by reading them from provided normalized graphs. Simple explicit formulas for the noise introduced by a switching pair are derived, and the upper frequency limit of validity of the analysis is examined. Although capacitive effects are neglected, the results are applicable up to the gigahertz frequency range for modern submicrometer CMOS technologies. The deviation of the device characteristics from the ideal square law is taken into account, and the analysis is verified with measurements.**

***Index Terms*—Active mixers, analog integrated circuits, CMOS analog integrated circuits, CMOS mixers, frequency conversion, Gilbert cell, mixer noise, mixers.**

I. Introduction

THE mixer or frequency converter is a significant noise contributor in most communication systems. Its function is inherently noisy because noise is transferred from multiple frequency bands to the output. Since the circuit performs frequency translation, it is not linear time-invariant and its noise behavior cannot be analyzed with conventional circuit techniques. This makes the designer almost exclusively dependent on nonlinear noise simulators [5], [18]. Fast estimation of the noise performance is desirable because this capability facilitates design optimization and accelerates the design cycle.

Active CMOS mixers in which a switching pair is used for current-commutation, such as the CMOS Gilbert cell, are commonly used in communication systems [1]–[4]. Modern CMOS processes are becoming widely used in the realization of communication circuits because they are capable of achieving high-frequency performance, are inexpensive, and are appropriate for a high level of integration. Active mixers have conversion gain, relaxing the gain requirements of the blocks preceding the mixer and the noise requirements of the blocks following it.

In this paper, we examine the operation and the noise performance of current-commutating active CMOS mixers, neglecting capacitive effects. The results are applicable when the mixer operates at moderate frequencies used at the intermediate-frequency (IF) stage of a receiver, or, considering modern submicrometer technologies and high bias current, at higher frequencies used at the radio-frequency (RF) front end. A corresponding noise analysis of bipolar active mixers has been presented in [6].

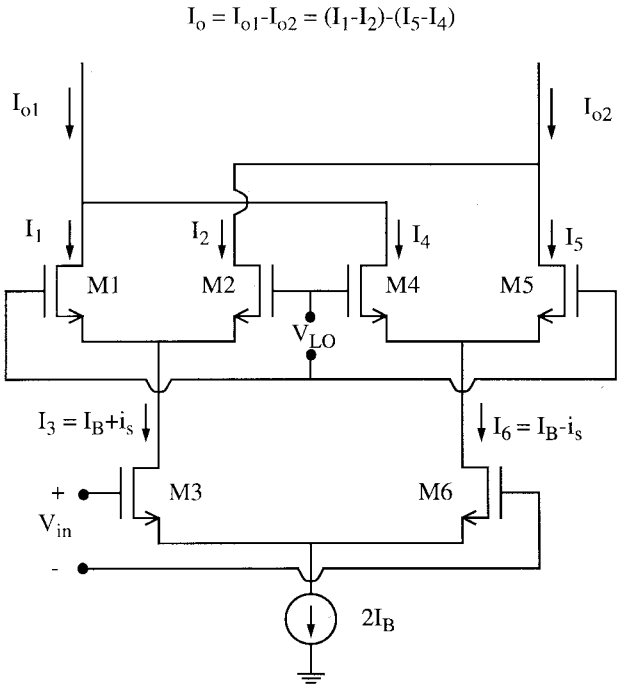

Fig. 1. A CMOS Gilbert cell.

The simple single-balanced active mixer is examined, and the results are also presented for the double-balanced circuit, the Gilbert cell. The analysis can be readily adapted for variations of the above structures, such as the current reuse configuration presented in [2], cases where the output is taken in single-ended form rather than differential, degeneration is employed to linearize the transconductance stage, or a matching network is used at the input.

II. The Gilbert Cell and the Single-Balanced Structure

The Gilbert cell, shown in Fig. 1, was initially designed with bipolar transistors [7] to operate as a precision multiplier, but it has been used widely as a mixer with the transistors driven by the strong local oscillator (LO) signal acting as switches. The operation principle is the same in CMOS technology. It is a doubly balanced mixer, meaning that if only one of the LO or input signals is applied, the output is ideally zero. The output signal ideally does not contain a component at the LO

Manuscript received June 1, 1998; revised January 4, 1999. This work was supported by the U.S. Army Research Office under Grant DAAG55-97-1-0340.

The authors are with the Electronics Research Laboratory, Department of Electrical Engineering and Computer Science, University of California, Berkeley, CA 94720 USA.

Publisher Item Identifier S 0018-9200(99)04202-X.

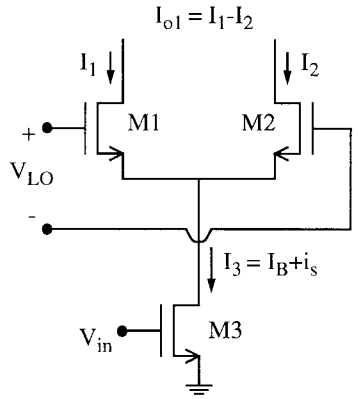

Fig. 2. A single-balanced active CMOS mixer.

frequency and its harmonics. There exists high port-to-port isolation among the input, LO, and output ports, alleviating problems such as LO leakage to the antenna and reducing the amount of output filtering required.

The Gilbert cell consists of a transconductance or driver stage, which is a differential pair biased at a fixed operating point, and two switching pairs driven by the strong LO signal. Resistive or tuned tank loads can be connected at the output, and degeneration can be used to linearize the transconductance stage. The output current is

$$I_o = I_{o1} - I_{o2} = (I_1 - I_2) - (I_5 - I_4) \tag{1}$$

where the above currents are defined in Fig. 1. If i_s is the small-signal current at one output branch of the driver stage, assuming ideal switching, during the first half of the LO period $I_o = 2i_s$, while during the other half $I_o = -2i_s$. This alternation in the sign of the output signal provides the desired mixing effect.

It will be helpful below to consider half a Gilbert cell, shown in Fig. 2. This circuit is a single-balanced mixer itself, meaning that the output current I_{o1} is zero when only an input signal is applied without the LO signal. The transconductance stage is a single transistor. From (1), the output of the Gilbert cell is the difference of the output currents of two single-balanced mixers, and therefore the results carry over easily from the single- to the double-balanced case.

III. Transistor Model and Switching Pair Large-Signal Equations

The simple square-law MOSFET model is not accurate for modern short-channel technologies, and a better approximation for the I–V relation of a MOS transistor is [8]

$$I = K\frac{(V_{\rm GS} - V_T)^2}{1 + \theta(V_{\rm GS} - V_T)}. \tag{2}$$

In (2), I is the drain current, $V_{\rm GS}$ is the gate-source voltage, and V_T is the threshold voltage of the device. Parameter K depends on the technology and the size of the device and is proportional to the channel width. Parameter θ models to a first order the source series resistance, mobility degradation due to the vertical field, and velocity saturation due to the lateral field in short-channel devices. It depends on the channel length and is independent of the body effect.

Since a large ac drive is applied to the switching pair, the bias of $M1$ and $M2$ is not fixed but varies periodically with time. When a differential voltage greater than a certain value V_x is applied between the gates of the two transistors, one of them switches off. When the absolute value of the instantaneous LO voltage $V_{\rm LO}$ is lower than V_x, the current of the driver stage is shared between the two devices. In this case, it is desirable to find the drain current of each transistor for a given LO voltage and driver-stage bias current. We will assume that the output conductance of the devices can be neglected, and therefore $M3$ can be modeled with an ideal current source I_B. We will also assume that the load of $M1$ and $M2$ is such that they remain in saturation during the part of the LO period that they are on.

The large-signal behavior of the switching pair is described by the system of two equations

$$K_1\frac{(V_{\rm GS1} - V_T)^2}{1 + \theta(V_{\rm GS1} - V_T)} + K_1\frac{(V_{\rm GS2} - V_T)^2}{1 + \theta(V_{\rm GS2} - V_T)} = I_B \tag{3}$$

and

$$V_{\rm GS1} - V_{\rm GS2} = V_{\rm LO} \tag{4}$$

where K_1 is the K parameter of $M1, M2$, and $V_{\rm GS1}, V_{\rm GS2}$ are the gate-source voltages of $M1, M2$. If we normalize I_B and $V_{\rm LO}$ as follows:

$$J_B = \frac{\theta^2}{K_1} I_B \tag{5}$$

$$U_{\rm LO} = \theta V_{\rm LO} \tag{6}$$

and also let

$$U_1 = \theta(V_{\rm GS1} - V_T) \quad U_2 = \theta(V_{\rm GS2} - V_T) \tag{7}$$

then (3) and (4) become

$$\frac{U_1^2}{1 + U_1} + \frac{U_2^2}{1 + U_2} = J_B \tag{8}$$

$$U_1 - U_2 = U_{\rm LO}. \tag{9}$$

Equations (8) and (9) can be transformed to one nonlinear equation with U_1 as the unknown, which can be solved rapidly with an iterative numerical method. Considering a positive $V_{\rm LO}$, the desired value of U_1 lies between $U_{\rm LO}$ and

$$\theta V_x = \frac{J_B}{2} + \sqrt{\frac{J_B^2}{4} + J_B} \tag{10}$$

which is the value of U_1 when the whole bias current passes through $M1$. With the transformation of (5) and (6), the normalized current of each transistor can be found in terms of J_B and $U_{\rm LO}$, independent of the technology parameters. For $M1$, for example

$$J_1 = \frac{\theta^2}{K_1} I_1 = \frac{U_1^2}{1 + U_1}. \tag{11}$$

The transconductance of each transistor will be needed below and can be calculated as the derivative of I with respect to $V_{\rm GS}$ from (2), or in normalized form as the derivative of J_1 with U_1 from (11).

It is worth noticing that no specific value of V_T is needed to calculate the drain current of $M1$ and $M2$. The behavior of the switching pair is independent of V_T and therefore to a first order is independent of the body effect and the common-mode LO voltage. This observation allows us to omit the small-signal body transconductance below.

In the following analysis, some performance parameters of the switching pair will be given in terms of the normalized bias current J_B and LO amplitude $U_o = \theta V_o$, with V_o being the real LO amplitude. The subthreshold conduction of the transistors has been neglected. Therefore, if the devices operate at very low current density, the prediction will be inaccurate, especially for low LO amplitude where the transistors do not act as switches and their behavior depends on their I–V characteristics.

IV. Deterministic Signal Processing

If capacitive effects are ignored, the output current of the single-balanced mixer of Fig. 2 is a function of the instantaneous LO voltage $V_{\rm LO}(t)$ and the current at the output of the driver stage $I_3 = I_B + i_s$, with I_B being the bias current and i_s the small-signal current

$$I_{o1} = I_1 - I_2 = F(V_{\rm LO}(t), I_B + i_s). \tag{12}$$

Since i_s is small, a first-order Taylor expansion gives

$$I_{o1} = F(V_{\rm LO}(t), I_B) + \frac{\partial}{\partial I_B} F(V_{\rm LO}(t), I_B) \cdot i_s \tag{13}$$

or

$$I_{o1} = p_0(t) + p_1(t) \cdot i_s. \tag{14}$$

Both $p_o(t)$ and $p_1(t)$ are periodic waveforms, depicted in Fig. 3. As can be seen from (1) and (14), in a doubly balanced structure with perfect device matching, $p_o(t)$ is eliminated. During the time interval Δ, when the LO voltage is between V_x and $-V_x$, and both transistors are on, $p_o(t)$ and $p_1(t)$ depend on $V_{\rm LO}(t)$, I_B, and the I–V characteristics of the transistors. The small-signal current in each branch is determined by current division, and one can see that

$$p_1(t) = \frac{g_{m1}(t) - g_{m2}(t)}{g_{m1}(t) + g_{m2}(t)} \tag{15}$$

where $g_{m1}(t)$ and $g_{m2}(t)$ represent the instantaneous small-signal transconductances of $M1$ and $M2$. According to (14), a signal component $x(t)$ of $i_s(t)$ is multiplied by the waveform $p_1(t)$, and therefore the frequency spectrum of the corresponding output is

$$Y_x(f) = \sum_{n=-\infty}^{\infty} p_{1,n} \cdot X(f - nf_{\rm LO}) \tag{16}$$

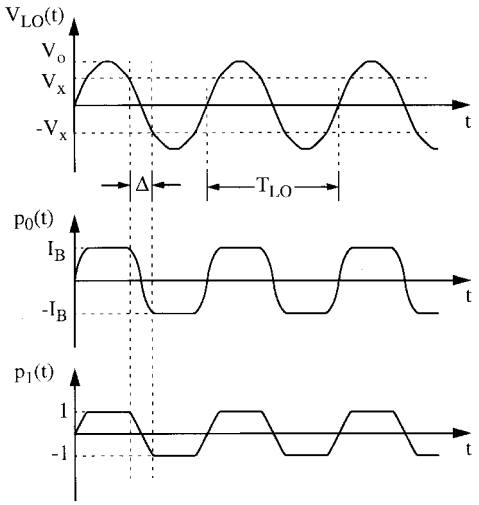

Fig. 3. Waveforms $p_o(t)$ and $p_1(t)$.

where $f_{\rm LO}$ is the LO frequency, $p_{1,n}$ are the Fourier components of $p_1(t)$, and $X(f)$ is the frequency spectrum of $x(t)$.

It is worth noticing that with good device matching, $p_1(t) = -p_1(t + T_{\rm LO}/2)$, with $T_{\rm LO}$ being the LO period, and hence $p_1(t)$ has only odd-order frequency components. The same observation can be made for $p_o(t)$.[1] Usually the term for $n = 1$ or $n = -1$ is of interest, corresponding to shifting up or down the input signal in the frequency domain by one multiple of the LO frequency, and in this case $c = |p_{1,1}| = |p_{1,-1}|$ represents the conversion gain of the switching pair alone. Since $x(t) = g_{m3} v_{\rm in}(t)$ where $v_{\rm in}(t)$ is the input voltage signal at the gate of $M3$ and g_{m3} is the transconductance of $M3$, the conversion gain of the single-balanced mixer in transconductance form is

$$g_c = c \cdot g_{m3}. \tag{17}$$

For high LO amplitude, $p_1(t)$ approaches a square waveform and c approaches $2/\pi$. Fig. 4 shows c, evaluated numerically as a function of the normalized bias current J_B and LO amplitude U_o, for a sinusoidal LO waveform. Assuming $V_o > V_x$, as it should be for proper mixer operation, an estimate for c can be obtained by approximating $p_1(t)$ with a straight line during Δ

$$c \cong \frac{2}{\pi} \left(\frac{\sin(\pi \Delta f_{\rm LO})}{\pi \Delta f_{\rm LO}} \right) \tag{18}$$

where for a sinusoidal LO waveform

$$\pi \Delta f_{\rm LO} = \arcsin\left(\frac{V_x}{V_o} \right) \tag{19}$$

and V_x is given by (10). Comparison with the numerically evaluated value of c for a sinusoidal LO waveform shows that

[1] For a similar reason, the results that the conversion gain to even-order sidebands is zero and that the strong signal output component contains only odd-order harmonics of the LO frequency also hold at high frequencies.

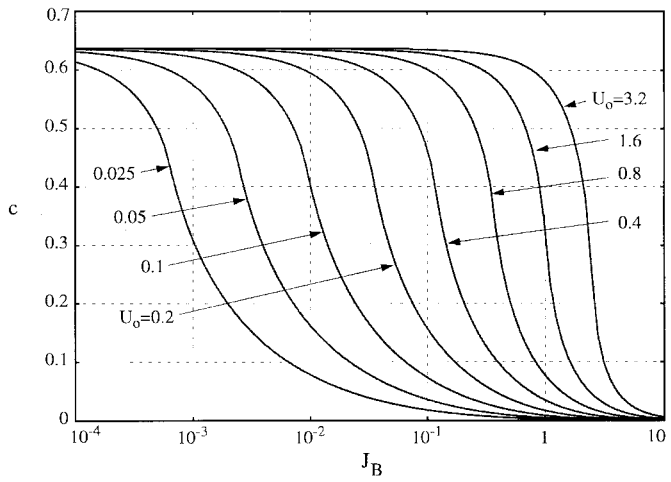

Fig. 4. Numerically evaluated conversion gain of the switching pair c.

(18) is a good approximation for low values of U_o, introducing error below 1 dB if $U_o < 0.7$. It overestimates c for higher values of U_o, introducing error below 2 dB if $U_o < 1.6$ and below 3.5 dB if $U_o < 3.2$.

It is easy to observe that the conversion gain of the Gilbert cell is also given by (17). If degeneration or an input matching network is used, the transconductance of the driver stage is not g_{m3} but can be calculated with linear circuit techniques and multiplied with c to provide the conversion gain.

V. Noise Analysis

There are two reasons why the noise generated in a mixer has periodically time-varying statistics. First, the operating point of the devices changes periodically with time. Second, the processing of the signal from the point at which noise is generated to the output can be periodically time-varying [6]. A random process whose statistics are periodic functions of time is called cyclostationary, and a complete description of such a process requires a time-varying power spectral density (PSD) $S(f,t)$ [17]. This is different from the wide sense stationary (WSS) noise generated by a linear time-invariant circuit.

Consider a device that with a fixed operating point produces shot or thermal white noise. It can be shown [18] that if the operating point changes with time, the resulting noise is still white, with a time-varying PSD given by the same formula as for the time-invariant case if we replace the value of the fixed resistor with the time-varying one for thermal noise and the value of the fixed current across the p-n junction by the time-varying one for the shot noise.

We will use the fact that the PSD of the drain current thermal noise generated by a MOS transistor in saturation is

$$\frac{\overline{i_n^2}}{\Delta f} = 4kT\gamma g_m \tag{20}$$

where g_m is the gate transconductance, k is Boltzmann's constant, T is the absolute temperature, and γ is 2/3 for long-channel transistors but can be higher for short channel devices, can depend on bias, and can be affected by hot electron phenomena [9]–[14].[2]

In the following analysis we will calculate the time-average noise at the output of the mixer, and based on that we will evaluate the noise figure.

A. Noise from the Driver Stage

Consider the noise component $n_3(t)$ of $i_s(t)$ in Fig. 2. This is considered to be WSS with PSD $S_{n3}(f)$ and can represent noise generated in $M3$ or noise present at the input of the mixer and amplified by $M3$. The output noise component that $n_3(t)$ contributes

$$y_{n3}(t) = n_3(t) \cdot p_1(t) \tag{21}$$

is cyclostationary, and its time-average PSD is

$$S_{n3}^o(f) = \sum_{n=-\infty}^{\infty} |p_{1,n}|^2 S_{n3}(f - nf_{\rm LO}). \tag{22}$$

Assuming that $n_3(t)$ is white over the bandwidth of interest, $S_{n3}(f)$ equals N_{n3}, a constant, and

$$S_{n3}^o(f) = N_{n3} \cdot \sum_{n=-\infty}^{\infty} |p_{1,n}|^2 = \alpha N_{n3} \tag{23}$$

where

$$\alpha = \sum_{n=-\infty}^{\infty} |p_{1,n}|^2 = \frac{1}{T_{\rm LO}} \int_0^{T_{\rm LO}} (p_1(t))^2 \, dt \tag{24}$$

is the power of waveform $p_1(t)$. Equations (23) and (24) can be used to find the noise contribution to the output without any assumptions about the LO waveform or amplitude.

For large LO amplitude, $p_1(t)$ approaches a square waveform, and its power α approaches one. It is interesting to examine the contribution of every individual sideband in the case of a square waveform. Noise from $f_{\rm LO} \pm f_{\rm out}$, with $f_{\rm out}$ being the output frequency, accounts for 81% of the noise transferred to the output, from $3f_{\rm LO} \pm f_{\rm out}$ for 9% and from all higher order sidebands together for 10%. Parameter α is evaluated numerically and given in Fig. 5 as a function of the normalized bias current J_B and LO amplitude U_o, for sinusoidal LO waveform. Similarly to the conversion gain of the switching pair c, if $V_o > V_x$, an estimate for α can be obtained by approximating $p_1(t)$ with a straight line during Δ

$$\alpha \cong 1 - \tfrac{4}{3}(\Delta f_{\rm LO}) \tag{25}$$

where for a sinusoidal LO waveform, $\Delta f_{\rm LO}$ can be obtained from (19). Comparison with the numerically computed value of α in the case of a sinusoidal LO waveform shows that (25) introduces error smaller than 25% if $U_o < 0.8$. It overestimates

[2] In the literature the drain current noise PSD in saturation is usually given by $\overline{i_n^2}/\Delta f = 4kT\gamma' g_{\rm do}$, where $g_{\rm do}$ is the small-signal drain-source conductance, for the same $V_{\rm GS}$ and $V_{\rm DS} = 0$ [10]–[14]. For long channel devices $g_m = g_{do}$ and (20) results, with $\gamma = \gamma' = 2/3$. For short channel devices γ' becomes a function of bias and is higher than 2/3. Therefore (20) results again with $\gamma = \gamma' \cdot (g_{do}/g_m) > 2/3$, a different function of bias than γ'.

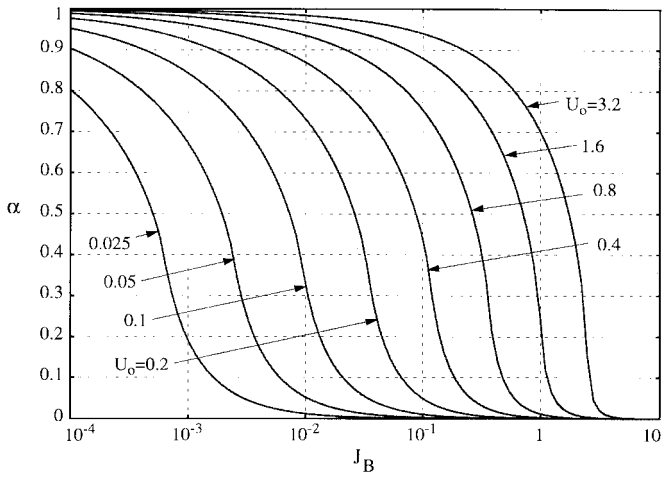

Fig. 5. Numerically evaluated average power α of waveform $p_1(t)$.

α by less than 50% if $U_o < 1.6$ and by less than 85% if $U_o < 3.2$.

For the single-balanced mixer, assuming that N_{n3} consists of the thermal noise of $M3$, the input source resistance R_s, and the polysilicon gate resistance r_{g3}, the noise transferred to the output is

$$S^o_{n3}(f) = \alpha \cdot 4kT\left(R_s + r_{g3} + \frac{\gamma}{g_{m3}}\right)g^2_{m3} \tag{26}$$

while for the Gilbert cell

$$S^o_{n,36}(f) = \alpha \cdot 4kT\left(R_s + 2r_{g3} + \gamma\frac{2}{g_{m3}}\right)g^2_{m3}. \tag{27}$$

If resistive degeneration is used, the noise at the output of the driver stage is white and (23) applies. If inductive degeneration or an impedance matching network is used, the gain of the driver stage is frequency dependent. The PSD of the noise at the output of the driver stage at the frequencies of interest—$f_{\rm LO} \pm f_{\rm out}, 3f_{\rm LO} \pm f_{\rm out}$, etc.—can be calculated with linear circuit techniques, and the output noise at $f_{\rm out}$ can be calculated from (22). Because of the frequency selective gain of the driver stage, possibly only a few sidebands need to be taken into account.

B. Thermal Noise Generated in the Switching Pair

We consider now thermal noise generated in $M1$ and $M2$ in Fig. 2, assuming that they remain in saturation during the part of the period that they are on. Neglecting capacitive effects and the output conductance of the transistors, when $M1$ or $M2$ is off, the output current is determined by I_3 and the switching pair does not contribute to the output noise. For this reason, when the LO amplitude is high, the noise contribution of the switching pair is usually lower than that of the driver stage. During the time interval Δ, both $M1$ and $M2$ are on and contribute to the output noise. The instantaneous noise PSD at I_1 is

$$4KT\gamma\left(\frac{1}{g_{m1}}\left(\frac{g_{m1}}{1+g_{m1}/g_{m2}}\right)^2 + \frac{1}{g_{m2}}\left(\frac{g_{m2}}{1+g_{m2}/g_{m1}}\right)^2\right) = 4kT\gamma\left(\frac{g_{m1}\cdot g_{m2}}{g_{m1}+g_{m2}}\right). \tag{28}$$

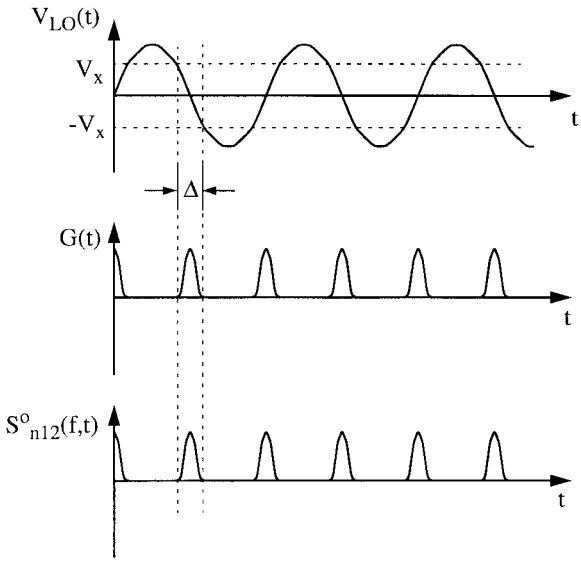

Fig. 6. Time-varying transconductance of the switching pair and time-varying PSD of the generated thermal noise.

Since the sum of I_1 and I_2 equals I_3, the amplitude of the noise component at the output I_{o1} is twice that at I_1, and the corresponding output noise PSD is

$$S^o_{n12}(f,t) = 16KT\gamma\left(\frac{g_{m1}\cdot g_{m2}}{g_{m1}+g_{m2}}\right) = 8kT\gamma G(t) \tag{29}$$

where

$$G(t) = 2\frac{g_{m1}\cdot g_{m2}}{g_{m1}+g_{m2}} \tag{30}$$

is the small-signal transconductance of the whole differential pair, from $V_{\rm LO}$ to I_{o1}. This time-varying PSD is flat in frequency since it represents white noise and is shown in Fig. 6. The peak of $S^o_{n12}(f,t)$ appears for $V_{\rm LO} = 0$ and is independent of the LO amplitude. The higher the LO amplitude, the smaller the time interval Δ and the lower the noise contribution to the output. From (29), we obtain the time-average PSD at the output

$$S^o_{n12}(f) = 8kT\gamma\left(\frac{1}{T_{\rm LO}}\int_0^{T_{\rm LO}} G(t)\,dt\right) = 8kT\gamma\overline{G} \tag{31}$$

where $\overline{G}$ is the time average of $G(t)$. This expression can be used to calculate $S^o_{n12}(f)$ without any assumptions about the LO waveform or amplitude. However, the LO amplitude is usually large, and a further simplification is possible. Assuming sinusoidal $V_{\rm LO}$ and changing the variable of integration from t to $V_{\rm LO}$, we obtain

$$\overline{G} = \frac{1}{\pi V_o}\int_{-V_x}^{V_x} G(V_{\rm LO})\frac{1}{\sqrt{1-(V_{\rm LO}/V_o)^2}}\,dV_{\rm LO}. \tag{32}$$

If the LO amplitude V_o is high, in the interval of integration $V_{\rm LO}$ is much smaller than V_o and $1/\sqrt{1-(V_{\rm LO}/V_o)^2} \approx 1$. In this case, since $G(V_{\rm LO}) = dI_{o1}/dV_{\rm LO}$, (32) provides

$$\overline{G} = \frac{1}{\pi V_o}\int_{-V_x}^{V_x}\left(\frac{dI_{o1}}{dV_{\rm LO}}\right)dV_{\rm LO} = \frac{2I_B}{\pi V_o}. \tag{33}$$

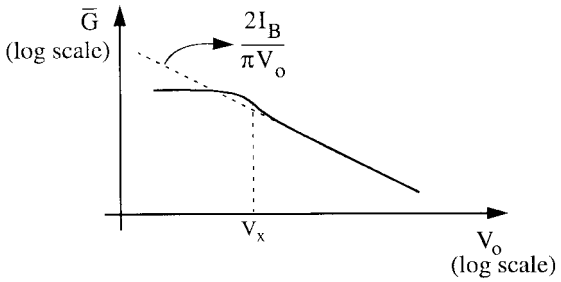

Fig. 7. Time-average transconductance of the switching pair $\overline{G}$ versus LO amplitude.

From (31) and (33), we obtain the contribution of the switching pair to the output noise

$$S^o_{n12}(f) = \frac{16kT\gamma}{\pi} \cdot \frac{I_B}{V_o}. \tag{34}$$

A sinusoidal LO signal was assumed above, but such a restriction is not necessary. A relation similar to (33) can be obtained directly from the definition of $\overline{G}$, only with the assumption of linear dependence of $V_{\rm LO}$ in t during the time interval Δ, with slope λ

$$\overline{G} = \frac{4}{T_{\rm LO}} \cdot \frac{I_B}{\lambda}. \tag{35}$$

For a sinusoidal LO waveform, $\lambda = 2\pi V_o/T_{\rm LO}$ and (33) results. Notice that no assumption was made about the I–V characteristics of the transistors and that (33)–(35) are independent of the transistor dimensions. These expressions, with $\gamma = 1/2$, can also be used for the time-average transconductance and the collector shot noise of a bipolar switching pair.

We observe that the PSD at the output is proportional to the bias current I_B and inversely proportional to the zero crossing slope of $V_{\rm LO}$. As can be seen in (32), if for moderate V_o the slope of $V_{\rm LO}(t)$ (proportional to $\sqrt{1-(V_{\rm LO}/V_o)^2}$) drops close to the ends of Δ, (33)–(35) slightly underestimate the output noise. For smaller V_o, $\overline{G}$ and $S^o_{n12}(f)$ approach the values that correspond to the fixed operating point of $V_{\rm LO} = 0$, and the above expressions overestimate the output noise, as demonstrated in Fig. 7. A graph of $(\theta/K_1)\overline{G}$ evaluated numerically as a function of J_B and U_o is given in Fig. 8 for a sinusoidal LO waveform. Comparison of the prediction of (33) with the computed value of $\overline{G}$ for a sinusoidal LO waveform shows that if $V_o > V_x$, then (33) underestimates $\overline{G}$ by less than 25% for all the values of U_o shown in Fig. 8, with the error growing as V_o approaches V_x. The output noise contribution of the two switching pairs of a Gilbert cell is twice that calculated for the single-balanced mixer.

Lacking a commonly accepted expression for γ as a function of bias, a fixed value was used above. In practice, the equations derived in this section can be used with the value of γ, which corresponds to the bias condition of $V_{\rm LO} = 0$. This is a reasonable approximation since the devices of the switching pair contribute the most noise for zero LO voltage.

C. Noise from the LO Port

Since the LO is a periodically time-varying circuit it is possible that the noise at its output contains a cyclostationary

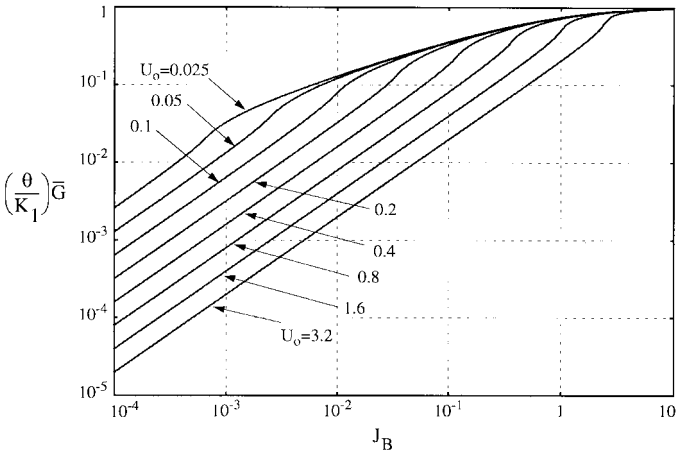

Fig. 8. Numerically evaluated time-average transconductance of the switching pair $\overline{G}$.

component. It is inaccurate to time-average its PSD and use it as if it were a WSS process, since the time-varying processing of this signal by the mixer tracks exactly the time variation of the noise statistics. Except for the case of white cyclostationary noise where time dependence of the PSD can be incorporated into the system [6], the treatment of such a problem is complicated and is described in [17]. Below we will consider the simplified case at which the noise present at the LO port is stationary. The results also apply to intrinsic noise of $M1$ and $M2$, which can be modeled with a time-invariant stationary voltage-noise source in series with the gates, such as thermal noise of the gate resistances and flicker noise discussed in Section V-E.

We assume that the LO voltage has a noise component $n_{\rm LO}(t)$. This contributes output noise

$$y_{n\rm LO}(t) = G(t)n_{\rm LO}(t) \tag{36}$$

where $G(t)$ is the time-varying transconductance of the switching pair defined in (30). If $n_{\rm LO}(t)$ is WSS with PSD $S_{n\rm LO}(f), y_{n\rm LO}(t)$ is a cyclostationary process with time-average PSD

$$S^o_{n\rm LO}(f) = \sum_{n=-\infty}^{\infty} |G_n|^2 S_{n\rm LO}(f - nf_{\rm LO}) \tag{37}$$

where G_n are the Fourier coefficients of the waveform $G(t)$.

If $n_{\rm LO}(t)$ is also white with PSD $S_{n\rm LO}(f) = N_{\rm LO}$, the noise contribution to the output becomes

$$S^o_{n\rm LO}(f) = N_{\rm LO} \cdot \sum_{n=-\infty}^{\infty} |G_n|^2 = \overline{G^2} \cdot N_{\rm LO} \tag{38}$$

where

$$\overline{G^2} = \left(\frac{1}{T_{\rm LO}} \int_0^{T_{\rm LO}} G(t)^2 \, dt \right). \tag{39}$$

With some manipulation, it can be shown that for LO amplitude fairly larger than V_x and square law equations

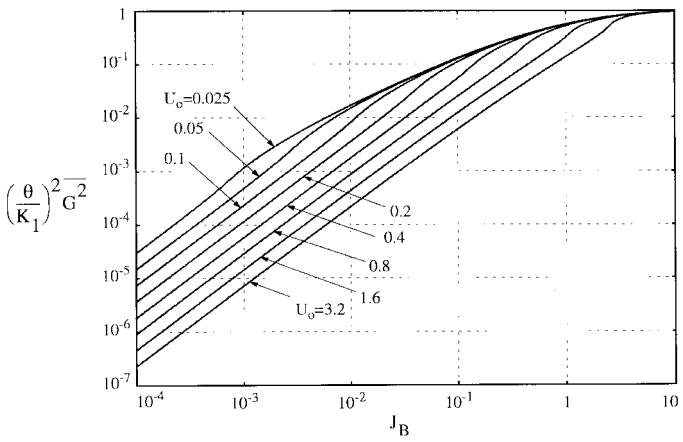

Fig. 9. Numerically evaluated time-average square transconductance of the switching pair $\overline{G^2}$.

$(\theta = 0)$

$$\overline{G^2} \approx 16\left(\frac{\ln(\sqrt{2}+1)}{\sqrt{2}} - \frac{1}{3}\right)\cdot\frac{K_1^{1/2}I_B^{3/2}}{\lambda T_{\rm LO}} = 4.64\cdot\frac{K_1^{1/2}I_B^{3/2}}{\lambda T_{\rm LO}} \tag{40}$$

where λ is as before the zero crossing slope of $V_{\rm LO}(t)$. A plot of $(\theta/K_1)^2\overline{G^2}$ as a function of the normalized bias current J_B and LO amplitude U_o, calculated numerically from (39), is shown in Fig. 9, assuming a sinusoidal LO waveform. Comparison of this computed value with the prediction of (40) derived for square-law equations shows that for $V_o > V_x$, (40) introduces error lower than 25% if $U_o < 0.8$. It overestimates $\overline{G^2}$ by less than 50% if $U_o < 1.6$ and less than 90% if $U_o < 3.2$.

For the single-balanced mixer, the white noise $N_{\rm LO}$ consists of the noise floor of the LO output spectrum, represented by an equivalent noise resistance $R_{\rm LO}$, and the thermal noise of the polysilicon gate resistance r_{g1} of the transistors

$$S_{n\rm LO}^o(f) = 4kT(R_{\rm LO} + 2r_{g1})\overline{G^2}. \tag{41}$$

The noise floor of the LO can significantly increase the noise figure of the mixer, and filters can be used to limit its effect. In a Gilbert cell, the external noise present at the LO port is rejected, and only the gate resistances contribute noise

$$S_{n\rm LO}^o(f) = 4kT(4r_{g1})\overline{G^2}. \tag{42}$$

D. Mixer Noise Figure

Having calculated the noise contribution from the various sources to the output, the noise figure of the mixer can be estimated. Consider that the load introduces output noise, which can be represented by an equivalent noise resistance R_L. The single-sideband (SSB) noise figure for the single-balanced mixer is as shown in (43) at the bottom of the page, and for the Gilbert cell is

$$({\rm NF})_{\rm SSB} = \frac{\alpha}{c^2} + \frac{2(\gamma_3 + r_{g3}g_{m3})g_{m3}\alpha + 4\gamma_1\overline{G} + 4r_{g1}\overline{G^2} + \dfrac{1}{R_L}}{c^2 g_{m3}^2 R_s} \tag{44}$$

where the quantities $\alpha, c, \overline{G}, \overline{G^2}$ are evaluated with the bias current of each switching pair and the symbols γ_1 and γ_3 have been used for the noise factor γ of $M1$ and $M3$, respectively. If a band-pass filter is used at the input (which filters out noise from the source resistor at frequencies outside the input signal band), the term α/c^2 in (43) and (44) becomes one. If the useful signal is present in both sidebands around the LO frequency, the double-sideband noise figure is the appropriate noise performance metric. For the single-balanced mixer and the Gilbert cell, this is half of the SSB noise figure given by (43) and (44), respectively. As in the SSB case, if a band-pass filter is used at the input to reject noise from the source resistor at frequencies outside the two input signal bands, the first term $\alpha/(2c^2)$ becomes one. Comparing the above equations and neglecting the noise from the LO port, we observe that for equal conversion gain, the double-balanced structure consumes twice the power of the single-balanced one and has a higher noise figure.

E. Flicker-Noise Effects

In the above analysis, the effect of flicker noise was neglected, but if the system employs direct conversion this can be a limiting factor. Flicker noise from the driver stage appears at the output around $f_{\rm LO}$ and all the odd-order harmonics, since, as discussed in Section IV, $p_1(t)$ has only odd-order frequency components. If the PSD of flicker noise is known at the output of the driver stage, the PSD at the output around $f_{\rm LO}$ can be easily found from (22), since the conversion gain of the switching pair $c = |p_{1,1}|$ has been calculated in Section IV.

To estimate the flicker-noise contribution from the switching pair, we need to know the flicker-noise behavior of MOS devices with time-varying operating point. Assuming that a usual time-invariant flicker-noise voltage source in series with the gate is an appropriate model, from (36) this noise is transferred to the output by multiplication with $G(t)$. It is easy to see in Fig. 6 that the period of $G(t)$ is $T_{\rm LO}/2$, and therefore it contains only even-order harmonics of the LO frequency. This means that flicker noise from the switching pair will appear at the output around dc but not around $f_{\rm LO}$. The PSD of the noise contribution of each transistor to the output around dc can be easily found from (37) since G_0 is the time-average transconductance of the switching pair $\overline{G}$, which has been calculated in Section V-B.

$$({\rm NF})_{\rm SSB} = \frac{\alpha}{c^2} + \frac{(\gamma_3 + r_{g3}g_{m3})g_{m3}\alpha + 2\gamma_1\overline{G} + (R_{\rm LO} + 2r_{g1})\overline{G^2} + \dfrac{1}{R_L}}{c^2 g_{m3}^2 R_s}. \tag{43}$$

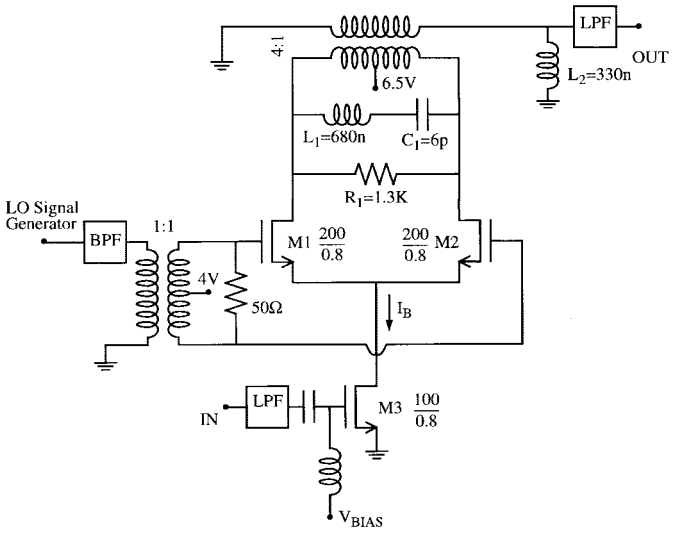

Fig. 10. Measurement setup of a single-balanced mixer.

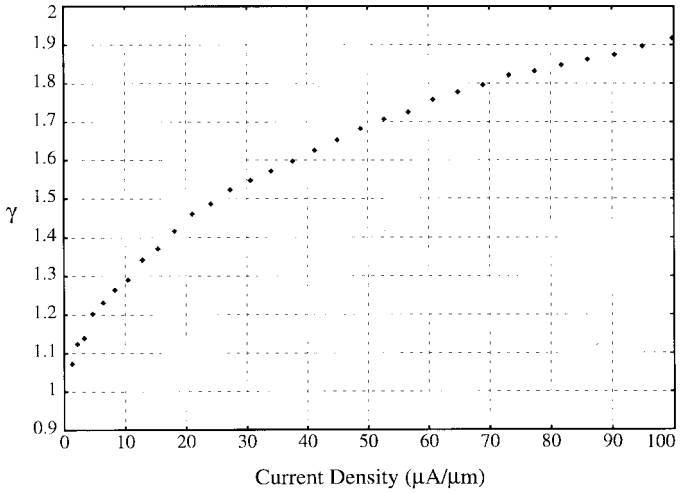

Fig. 11. Extracted γ versus current density for a minimum channel length Qubic2 MOS transistor.

VI. Measurements

The SSB noise figure of a single-balanced mixer shown in Fig. 10, fabricated in the Philips Qubic2 process, with minimum drawn length 0.8 μ, was measured at low frequencies. The drains of $M1$ and $M2$ were brought off chip. No attempt was made to optimize its performance, the goal being to compare predictions with measurements. No input matching was used that would improve conversion gain and lower the noise figure. The measurements were taken with the noise-figure meter HP8970A [15].

Baluns with a center tap were used to transform the differential output signal to single ended and the single-ended LO signal to differential. The series L_1–C_1 trap was used to null the strong LO component at the output, which could saturate the noise-figure-meter input and drive $M1$ and $M2$ to the triode region. A band-pass filter reduced the noise floor of the LO signal. Care was taken to avoid introducing noise from the bias circuit.

The noise-figure meter measures its own noise figure with a 50-Ω source impedance during calibration and uses this measurement to extract the noise figure of the device under test (DUT). Therefore, the output impedance of the DUT must also be matched to 50 Ω, and inductor L_2 and resistor R_1 were used for this purpose. The board and balun parasitics significantly affect the behavior of the output load. It was measured that the trap resonance frequency is 72 MHz, used as LO frequency, and that an output parallel *RLC* resonance appears at 19 MHz, used as IF, with an impedance close to 50 Ω across the 4-MHz bandwidth that HP8970A measures noise. The output impedance of $M1$ and $M2$ is high in the bias condition of Fig. 10 and does not significantly affect the output impedance of the circuit.

During the measurements, the need to characterize individual components of the circuit arose. By connecting the gate of $M2$ to ground and the gate of $M1$ to a fixed bias, a cascode linear amplifier was formed. Its gain and noise figure were measured with a 50-Ω ac load at 19 MHz, and g_m and γ of $M3$ as a function of bias were extracted. To characterize the output load of Fig. 10, which was affected by the parasitics, this was used as a load of the linear amplifier, and the gain and noise-figure measurements were repeated. A second estimate for γ was obtained, which essentially coincided with the previous one. The effect of gate resistance noise [16] was removed, and the result is shown in Fig. 11. Parameter γ was found to depend on the bias current, but not significantly on the drain or body voltage, and therefore this measured value of γ versus bias current density was also used for the transistors of the switching pair.

The I–V curve of $M3$ was measured, and the parameters $\theta = 0.669$ V^{-1} and $K = 7.97$ mA/V^2 were extracted with curve fitting. These values were used to calculate the bias condition and small-signal transconductances of the transistors. For the transistors of the switching pair, the value of γ that corresponds to zero LO voltage was used. The predicted (computed numerically) and measured values for the noise figure and conversion gain are shown in Fig. 12, in which fairly good agreement is observed. It is worth noticing that because of the noise of the switching pair, the optimum noise figure appears for lower current than the optimum gain. The discrepancy is mainly because of the conversion gain prediction and can be attributed to the fact that the LO amplitude applied to the switching pair can be estimated but is not exactly known because of the losses in the band-pass filter, the balun, and the connections, and also to the fact that the transistor model used is inaccurate for low current density.

We will now elaborate on the calculation of the noise figure for one point of Fig. 12, namely, for $V_o = 1$ V and $I_B = 5.6$ mA, which corresponds to maximum conversion gain. Table I shows the numerically computed value of the parameters needed in the evaluation of the noise figure, together with the value resulting from approximate closed-form expressions derived in this paper. Table II shows the contribution of individual components of the circuit to the output noise.

VII. Upper Frequency Limit of the Analysis

To estimate the frequency range of validity of this noise analysis, it is necessary to consider the most significant of

TABLE I
PARAMETERS USED IN THE CALCULATION OF NOISE FIGURE FOR THE MIXER OF FIG. 10. $V_o = 1$ V AND $I_B = 5.6$ mA

Parameter	Numerically Evaluated	Closed-form Expression	
c	0.539	0.570	from (18), V_x=0.722V
a	0.590	0.658	from (25)
$\overline{G}$	3.84 (mA/V)	3.57 (mA/V)	from (33)
$\overline{G^2}$	32.7 (mA/V)^2	39.1 (mA/V)^2	from (40)

TABLE II
NOISE CONTRIBUTION FROM INDIVIDUAL COMPONENTS OF THE MIXER OF FIG. 10. $V_o = 1$ V AND $I_B = 5.6$ mA

Noise Contributors	Additional Information	Output Noise Power (pA^2/Hz)
R_s=50Ω	g_{m3}=7.98mA/V	15.2
R_L=276Ω		59.6
M3, r_{g3}=3.3Ω	γ_3=1.72	135.6
M1-M2	γ_1=1.36 (for V_{LO}=0)	172.1
R_{LO}=50Ω, r_{g1}=r_{g2}=6.6Ω		34.1

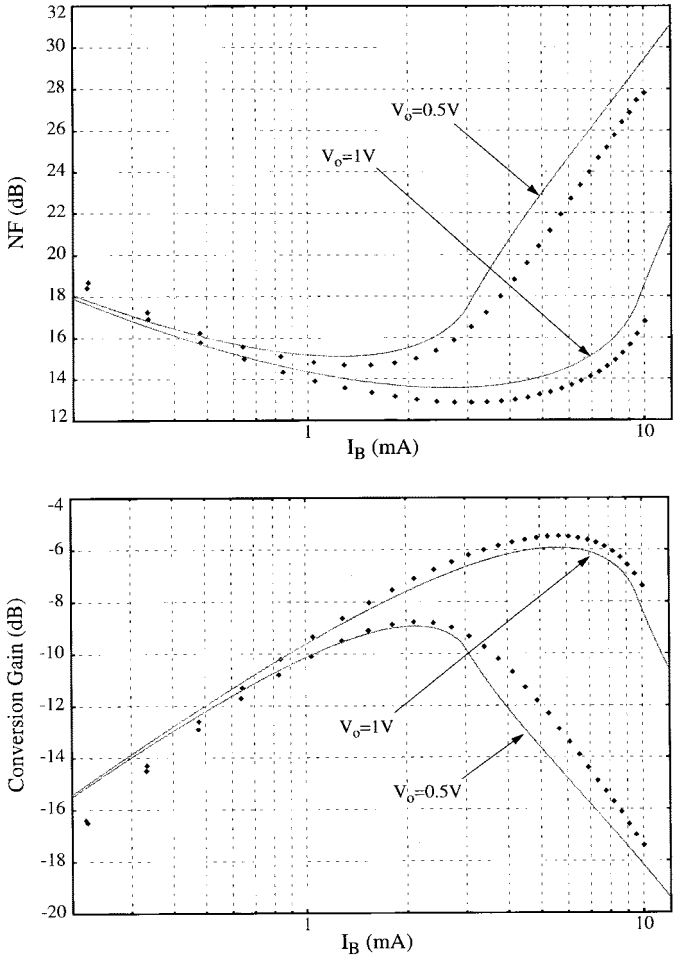

Fig. 12. Measured (dots) and predicted (solid line) noise figure and conversion gain of the single-balanced mixer of Fig. 10 versus bias current.

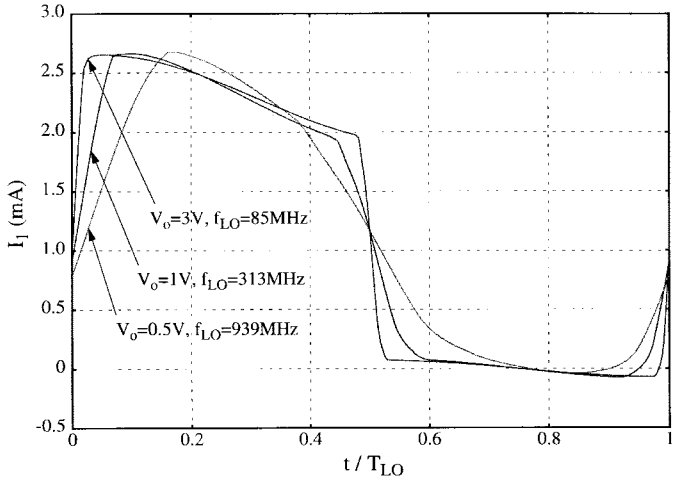

Fig. 13. Simulated drain current of $M1$ of the mixer of Fig. 10 over one LO period, for three different LO amplitudes, and LO frequencies given by (45) with $\varepsilon_1 = 0.3$. The bias current is $I_B = 2.3$ mA.

the transistor capacitances. Let C_1 and C_2 represent the gate-source capacitances of $M1$ and $M2$ and C_b denote the total capacitance from the common source node to the ground, consisting of the source-body capacitances of $M1$ and $M2$ and the drain-body capacitance of $M3$.

For this analysis to hold, reactive effects must not significantly alter the periodically varying operating point considered in Section III. It is shown in the Appendix that assuming a sinusoidal LO waveform and dc common LO voltage, an approximate upper LO frequency limit for this to hold is

$$f_{LO1} = \varepsilon_1 \frac{I_B}{2\pi(C_1 + C_2 + C_b)\left[\dfrac{V_o}{2} - (V_{gs1} - V_{gs0})\right]} \quad (45)$$

where ε_1 is a small number (e.g., 0.2 or 0.3), V_{gs1} and V_{gs0} are the low-frequency gate-source voltage of $M1$ for peak and zero LO voltage, respectively, and the sum of the capacitances is evaluated for zero LO voltage. It is interesting to observe

that high LO amplitude lowers this limit. Simulation with SpectreRF shows that (45) correctly predicts the LO frequency at which the operating point departs from the low-frequency behavior. Fig. 13 shows simulation results for the drain current of transistor $M1$ of the mixer of Fig. 10, for $I_B = 2.3$ mA, and for three different LO amplitudes, at the LO frequency $f_{\rm LO1}$ $(\varepsilon_1 = 0.3)$. The sum of the three capacitances was estimated from the available SPICE model to be 0.936 pF. To avoid reactive effects at the output, the drains of $M1$ and $M2$ were connected directly to the positive supply. In the three cases we observe approximately equal overshoot above 2.3 mA, which is the peak value of I_1 at low frequencies, and therefore about equal deviation from the corresponding low-frequency waveforms.

In addition, the small-signal conductance represented by the capacitors C_1, C_2, and C_b must be much lower than the sum of the conductances g_{m1} and g_{m2}. Otherwise, the signal is lost in these capacitors, while the switching pair contributes noise even if one of the transistors is off. For a down-conversion mixer in which the signal and the image frequencies are close to $f_{\rm LO}$, a second approximate upper LO frequency limit is

$$f_{\rm LO2} = \varepsilon_2 \frac{(g_{m1} + g_{m2})}{2\pi(C_1 + C_2 + C_b)} \tag{46}$$

where the sums of the capacitances and the conductances are considered constant and equal to their values for $V_{\rm LO}(t) = 0$ and ε_2 is again a small number (e.g., 0.2).

Simulation shows that for LO frequency below $f_{\rm LO2}$, the conversion gain and the noise figure are not significantly deteriorated by the change in operating point that occurs after $f_{\rm LO1}$ and that in some cases they improve. For $f_{\rm LO}$ higher than $f_{\rm LO2}$, the conversion gain and noise figure gradually degrade. Fig. 14 shows simulation results versus $f_{\rm LO}$ for the conversion gain, noise figure, and noise contribution of the switching pair of the mixer of Fig. 10 for three different LO amplitudes, together with the frequencies $f_{\rm LO1}$ $(\varepsilon_1 = 0.3)$ and $f_{\rm LO2}$ $(\varepsilon_2 = 0.2)$. The bias current is 2.3 mA, the input signal frequency is $1.1 f_{\rm LO}$, and the output signal frequency is $0.1 f_{\rm LO}$. For simplicity, the filters shown in Fig. 10 were not included in simulation. Ideal baluns where employed and the output stage consisted only of the balun. Since the output is obtained at low frequencies, reactive effects at the output do not affect the conversion gain. We observe that for large LO amplitude, the noise contribution of the switching pair does increase after $f_{\rm LO1}$, but in this case the switching pair is a minor contributor to the noise figure, which remains approximately constant up to $f_{\rm LO2}$. The slight noise increase at low frequencies is caused by flicker noise of the switching pair converted to baseband.

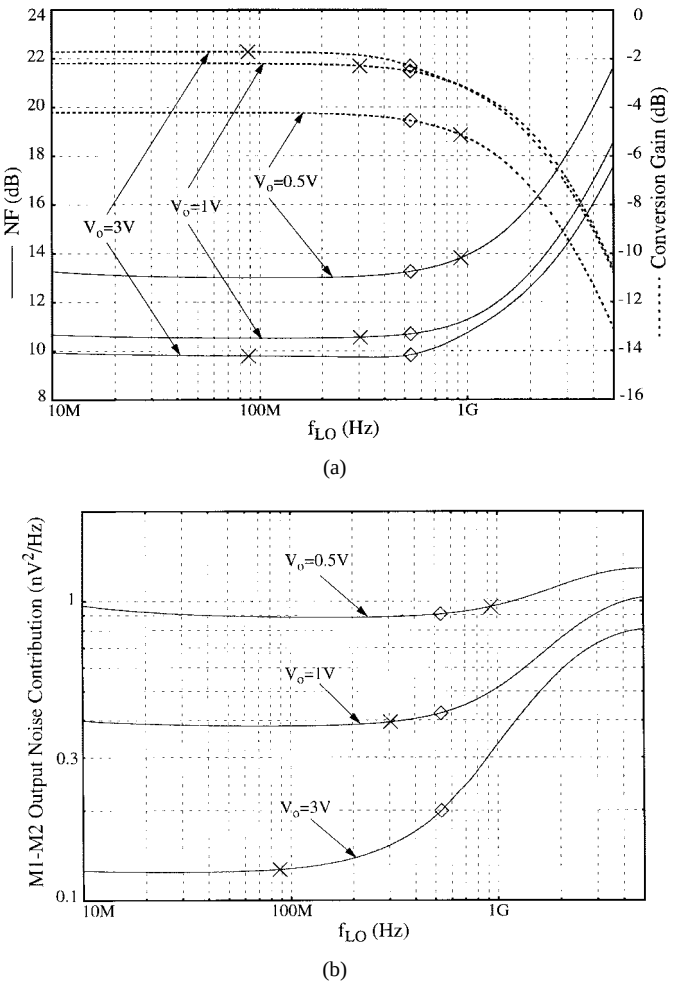

Fig. 14. (a) Noise figure and conversion gain and (b) switching pair output noise contribution versus frequency for the mixer of Fig. 10. Frequencies $f_{\rm LO1}$ (X) with $\varepsilon_1 = 0.3$ and $f_{\rm LO2}$ (diamonds) with $\varepsilon_2 = 0.2$ are shown.

VIII. Conclusions

A systematic study of the noise-generating mechanisms in current commutating CMOS mixers has been completed, and analytical expressions for important parameters have been derived. We can now comment on the effect of the design parameters on the noise performance.

High bias current improves the driver-stage transconductance and therefore the conversion gain and noise figure, provided that the LO amplitude and the size of the transistors of the switching pair are such that complete commutation is performed. As seen from (45) and (46), the use of high current density causes reactive effects to appear at higher frequencies.

Large LO amplitude increases the conversion gain and reduces the noise contribution of the switching pair and the LO port. After a certain value, the conversion gain of the switching pair reaches its maximum value $2/\pi$, the noise contribution of the switching pair becomes negligible, and further increase does not reduce the noise figure considerably. Large LO amplitude also allows operation at higher frequencies because complete current commutation can then be achieved with small-channel-width devices operating at high current density.

Increasing the channel width of $M1$ and $M2$ is desirable up to the point that for the given LO amplitude, c approaches $2/\pi$ and (34) and (40) hold. Further increase does not reduce the noise introduced by the switching pair as shown in (34), and it even increases the noise coming from the LO port as seen in (40). In addition, it introduces higher capacitances, which cause high-frequency deterioration in performance and represent a larger load for the LO. Increasing the channel width of $M3$ is desirable because this increases g_{m3} and therefore the conversion gain and reduces the noise figure. However,

large channel width of $M3$ introduces parasitic capacitance, which can degrade the performance at high frequencies and can represent a large load for the circuit driving the mixer.

Minimum channel length is preferred for the switching pair because increasing this reduces the conversion gain. Longer channel length requires larger channel width for operation with similar LO amplitude and bias current, which introduces higher parasitic capacitances. Minimum channel length is also appropriate for the driver stage since this maximizes the driver-stage transconductance. However, for longer channel devices, the noise factor γ of the transistors is closer to the ideal value of 2/3. Without an expression of γ as a function of channel length, it is difficult to quantify this benefit.

APPENDIX

We derive here a limit for the frequency-independent operating-point assumption used in the analysis. The high-frequency, large-signal equation for the switching pair is

$$I_B = I_1+I_2+C_1(V_1)\frac{dV_1}{dt}+C_2(V_2)\frac{dV_2}{dt}+C_b(V_{\rm bs})\frac{dV_{\rm bs}}{dt} \quad (47)$$

where $V_1, V_2, V_{\rm bs}$ are the voltages across capacitors C_1, C_2, C_b, respectively. We assume that the LO common voltage is constant with time and equal to $V_{{\rm LO},c}$. The voltages $V_1, V_2, V_{\rm bs}$ can be expressed as

$$V_1 = V_{{\rm LO},c} + \frac{V_{\rm LO}(t)}{2} - V_s \quad (48)$$

$$V_2 = V_{{\rm LO},c} - \frac{V_{\rm LO}(t)}{2} - V_s \quad (49)$$

$$V_{\rm bs} = -V_s \quad (50)$$

where $V_{\rm LO}(t)$ is the LO voltage and V_s the potential of the common source of $M1$ and $M2$. Using (48)–(50), (47) becomes

$$I_B = I_1+I_2+\frac{1}{2}(C_1-C_2)\frac{V_{\rm LO}}{dt}-(C_1+C_2+C_b)\frac{dV_s}{dt}. \quad (51)$$

Of the two terms involving capacitances in this equation, the last one is more significant and the other one is neglected. We will now estimate the maximum value of the derivative dV_s/dt, assuming a sinusoidal $V_{\rm LO}(t)$. At frequencies that the reactive effects are negligible, $V_s(t)$ is a periodic waveform with frequency $2f_{\rm LO}$, high voltage appearing when the LO voltage takes its peak value

$$V_{\rm sh} = V_{{\rm LO},c} + \frac{V_o}{2} - V_{\rm gs1} \quad (52)$$

and low voltage appearing when the LO voltage is zero

$$V_{s1} = V_{{\rm LO},c} - V_{\rm gs0} \quad (53)$$

where voltages $V_{\rm gs1}$ and $V_{\rm gs0}$ are the low-frequency gate-source voltages of $M1$ for $V_{\rm LO}(t) = V_o$ and $V_{\rm LO}(t) = 0$, respectively. Approximating $V_s(t)$ with a sinusoid, its maximum derivative is

$$\begin{aligned}\max\frac{dV_s}{dt} &= 2\pi(2f_{\rm LO})\frac{1}{2}(V_{sh}-V_{s1})\\ &= 2\pi f_{\rm LO}\left[\frac{V_o}{2}-(V_{\rm gs1}-V_{\rm gs0})\right]. \end{aligned} \quad (54)$$

Capacitances C_1, C_2, and C_b are voltage dependent, but we will make the approximation that their sum is constant and equal to its value for $V_{\rm LO} = 0$. From (51), for low-frequency behavior to hold, it must be

$$(C_1+C_2+C_b)\frac{dV_s}{dt} \ll I_B \quad (55)$$

and using (54), (45) results.

ACKNOWLEDGMENT

The authors wish to acknowledge that this work was accomplished in part at Texas Instruments, Dallas, TX, during the summer of 1996. Philips Semiconductors fabricated the test structures. The authors are grateful to K. McAdams of Philips Semiconductors for providing technical support during the measurements.

REFERENCES

[1] J. C. Rudell, J. J. Ou, T. B. Cho, G. Chien, F. Brianti, J. A. Weldon, and P. R. Gray, "A 1.9 GHz wide-band IF double conversion CMOS receiver for cordless telephone applications," *IEEE J. Solid-State Circuits*, vol. 32, pp. 2071–2088, Dec. 1997.

[2] A. N. Karanicolas, "A 2.7-V 900-MHz CMOS LNA and mixer," *IEEE J. Solid-State Circuits*, vol. 31, pp. 1939–1944, Dec. 1996.

[3] A. Rofougaran, J. Y.-C. Chang, M. Rofougaran, and A. A. Abidi, "A 1 GHz CMOS RF front-end IC for a direct conversion wireless receiver," *IEEE J. Solid-State Circuits*, vol. 31, pp. 880–889, July 1996.

[4] P. J. Sullivan, B. A. Xavier, and W. H. Ku, "Low voltage performance of microwave CMOS Gilbert cell mixer," *IEEE J. Solid-State Circuits*, vol. 32, pp. 1151–1155, July 1997.

[5] R. Telichevesky, K. Kundert, and J. White, "Receiver characterization using periodic small-signal analysis," in *Proc. Custom Integrated Circuits Conf.*, 1996, pp. 449–452.

[6] C. Hull, "Analysis and optimization of monolithic RF downconversion receivers," Ph.D. dissertation, Univ. of California, Berkeley, 1992.

[7] B. Gilbert, "A precise four quadrant multiplier with subnanosecond response," *IEEE J. Solid-State Circuits*, vol. SC-3, Dec. 1968, pp. 365–373.

[8] P. R. Gray and R. G. Meyer, *Analysis and Design of Analog Integrated Circuits*, 3rd ed. New York: Wiley, 1993.

[9] K. Takagi and A. Van der Ziel, "Excess high frequency noise and flicker noise in MOSFET's," *Solid-State Electron.*, vol. 22, pp. 289–292, 1979.

[10] A. A. Abidi, "High-frequency noise measurements on FET's with small dimensions," *IEEE Trans. Electron Devices*, vol. ED-33, pp. 1801–1805, Nov. 1986.

[11] B. Wang, J. R. Hellums, and C. G. Sodini, "MOSFET thermal noise modeling for analog integrated circuits," *IEEE J. Solid-State Circuits*, vol. 29, pp. 833–835, July 1994.

[12] D. P. Triandis, A. N. Birbas, and D. Kondis, "Thermal noise modeling for short-channel MOSFET's," *IEEE Trans. Electron Devices*, vol. 43, pp. 1950–1955, Nov. 1996.

[13] R. P. Jindal, "High frequency noise in fine line NMOS field effect transistors," in *Proc. IEDM*, 1985, pp. 68–71.

[14] S. Tedja, J. Van der Spiegel, and H. H. Williams, "Analytical and experimental studies of thermal noise in MOSFET's," *IEEE Trans. Electron Devices*, vol. 41, pp. 2069–2075, Nov. 1994.

[15] H. L. Swain and R. M. Cox, "Noise figure meter sets records for accuracy, repeatability, and convenience," *Hewlett-Packard J.*, pp. 23–24, Apr. 1983.

[16] B. Razavi, R.-H. Yan, and K. F. Lee, "Impact of distributed gate resistance on the performance of MOS devices," *IEEE Trans. Circuits Syst. I*, vol. 41, pp. 1505–1509, Nov. 1994.

[17] W. A. Gardner, *Introduction to Random Processes with Applications to Signals and Systems*, 2nd ed., McGraw Hill, 1989.

[18] A. Demir, "Analysis and simulation of noise in nonlinear electronic circuits and systems," Ph.D. dissertation, Univ. of California, Berkeley, 1997.

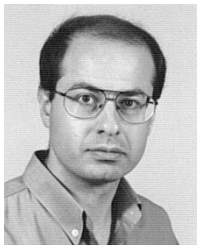

Manolis T. Terrovitis (S'94) was born in Athens, Greece, in 1969. He received the undergraduate diploma in electrical engineering from the National Technical University of Athens in 1992. He received the M.S. degree from the University of California at Berkeley in 1996, where he currently is pursuing the Ph.D. degree in the area of analog high-frequency integrated circuits for telecommunications.

He has held several short-term positions in the electronics industry, working on design and simulation issues of analog and mixed-signal circuits. He was with INTRACOM, Greece, in 1993, and he held summer internships at Texas Instruments, Dallas, TX, in 1996 and at Cadence Design Systems, San Jose, CA, in 1997 and 1998. His current interests include design and analysis of RF transceiver blocks in CMOS and bipolar technologies, device noise characterization, noise simulation of mixed-signal circuits, and communication system architectures.

Robert G. Meyer (S'64–M'68–SM'74–F'81), for a photograph and biography, see this issue, p. 771.